Characterization of the dynamic behavior of a diving board using motion capture data

Louise Demestre, Stéphane Grange, Cécile Dubois, Nicolas Bideau, Guillaume Nicolas, Charles Pontonnier, Georges Dumont

Characterization of the dynamic behavior of a diving board using motion capture data

Louise Demestre[1*], Stéphane Grange[2†], Cécile Dubois[1†], Nicolas Bideau[3†], Guillaume Nicolas[3†], Charles Pontonnier[1†] and Georges Dumont[1†]

[1*]Univ Rennes, Inria, IRISA - UMR 6074, Rennes, 35000, France.
[2]Univ Lyon, INSA-Lyon, GEOMAS, Villeurbanne, 69100, France.
[3*]Univ Rennes, Inria, M2S, Rennes, 35000, France.

*Corresponding author(s). E-mail(s):
louise.demestre@ens-rennes.fr;
Contributing authors: stephane.grange@insa-lyon.fr;
cecile.dubois@ens-rennes.fr; nicolas.bideau@univ-rennes2.fr;
guillaume.nicolas@univ-rennes2.fr; charles.pontonnier@irisa.fr;
georges.dumont@irisa.fr;
†These authors contributed equally to this work.

Abstract

The interaction between a diver and a diving board is one of the key factors of springboard diving performance. An accurate modelling of this interaction could provide new tools to better understand springboard diving performance. This study presents a finite element model of a springboard driven by motion capture data. The aim was to identify springboard mechanical parameters allowing to obtain a model with a mechanical behaviour similar to that observed experimentally. The mechanical characterization method was based on motion capture data of the diver and the springboard. Firstly, these data were used to estimate the interaction forces and moments between the diver and the springboard using an optimization approach. The interaction forces and moments were then applied to the springboard model to be characterized. Finally, the model parameters were identified minimizing the discrepancy between the experimental and numerical vertical displacements of the springboard. The best model obtained from this method led to a maximal mean absolute error between the

experimental and numerical vertical displacements between 0.045 m and 0.060 m. An accurate model may help to better understand energy transfers and time synchronisation between the diver and the springboard, which are key points of the diving board performance.

Keywords: Finite elements, human-structure interaction, sport performance, optimization

1 Introduction

According to the starting position, two kinds of dives can be achieved:

- dives with a starting position at the diving board free end (SP);
- dives with a running approach (RA) that includes the different phases presented in the Fig. 1.

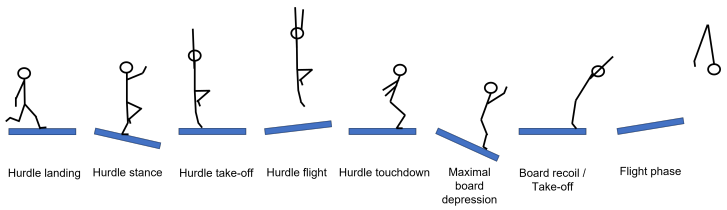

Fig. 1 Phases of a RA dive (c.f. [1, 2])

The diving judgement is based on the technique and grace of the starting position and the approach, the take-off, the flight and the entry into water. The degree of difficulty of the dive, which is multiplied by the judges' score, depends on the position of the diver in the air, the number of achieved somersaults and twists and the dive group (forward, reverse, backward, inward) [3]. The current study presents a diving board model and its mechanical characterization, taking into account the interaction with the diver throughout the dive. The characterization method is based on an optimization approach minimising the discrepancy between the experimental and numerical vertical displacements (E&NVD) of the diving board.

Previous studies aimed at better understanding how to maximize dive height or number of rotations or both. References [4, 5] mostly studied motor strategy during the flight phase. References [2, 5–7] focused on the take-off phase during which the diver is generating the angular momentum required for rotations during the flight phase and the horizontal velocity required for clearing the board [8, 9]. For RA dives, the diver has to make functional adjustments to adapt their motor behaviour to the hurdle step and take-off variability [1, 6, 10]. The diver's motion during the hurdle step and the board depression

is crucial to maximize the energy stored in the diving board [2, 7, 8, 11]. Therefore, the springboard diving performance depends on the interaction between the diver and the diving board throughout the dive. A better understanding of the dynamic behavior of the diving board is crucial in studying this performance.

Diving board models have been featured in the literature. Reference [12] found that a mass-spring system without damping was sufficient to model the static and dynamic behaviours of the diving board free end for given fulcrum setting and load location. Static trials were performed to determine the stiffness of the model using Hooke's law. Free oscillation trials with accelerometers located at different distances from the diving board free end were carried out to determine effective mass and damping. Reference [13] used this model to determine the natural frequency of the diving board studied. Reference [14] proposed a procedure based on dynamic trials to improve the diving board stiffness estimation. This model was then improved to allow springboard elements to tilt and thus produce a horizontal component of force on the diver's feet [7]. Reference [15] also improved the initial model adding damped oscillations coming from the fulcrum rebound. Reference [16] compared the initial model with two others: a discrete lumped-parameter model and a rigid beam model with a rotational spring at the origin, both without fulcrum detachment. The discrete lumped-parameter model was the most accurate but it had the highest computational cost. It was shown that the mass-spring system must be used only for cases with small deflections. The beam model was presented as a good compromise between accuracy and computational cost, especially when considering a coupling with a biomechanical model of a diver. Effective mass and stiffness of the beam were determined using trials performed in reference [12] and energies expressions. References [8, 9] used the rigid beam model linked to a 4-segment diver model at its free end to compute optimal standing jumps. Reference [17] modelled the diving board as a uniform beam with three degrees of freedom in the plane. The vertical displacement was modelled following the model from reference [12]. The horizontal and angular displacements were expressed as functions of the vertical displacement of the diving board free end. A planar 8-segment diver model was linked to the diving board free end. References [1, 6, 18] used this model to study the take-off phase.

Reference [2] recommended energy transfer studies during the dive. These energy transfers can be optimized by improving diver technique on the springboard [11]. The current study aimed at developing a finite element model of a diving board to study energy transfers and time synchronization between the diver and the diving board. This model takes into account the fulcrum setting, which impacts the springboard stiffness [8, 19]. Some assumptions were made to simplify the diving board modelling: constant thickness, full rectangular section, no perforations at the diving board free end (which is not the case on a real diving board [12]). We hypothesized that the presented method enables to obtain a characterized model (material, geometry and contact parameters) with a dynamic behaviour similar to the experimental one.

Firstly, the procedure to obtain experimental data is presented. Secondly, the different steps to simulate the dynamic behaviour of the diving board are detailed. Thirdly, the method to characterize the diving board model is presented. Finally, the accuracy of the characterization method is assessed.

A statistical analysis of the characterization method and an analysis of the discrepancy between the E&NVD are presented and then discussed.

2 Methods

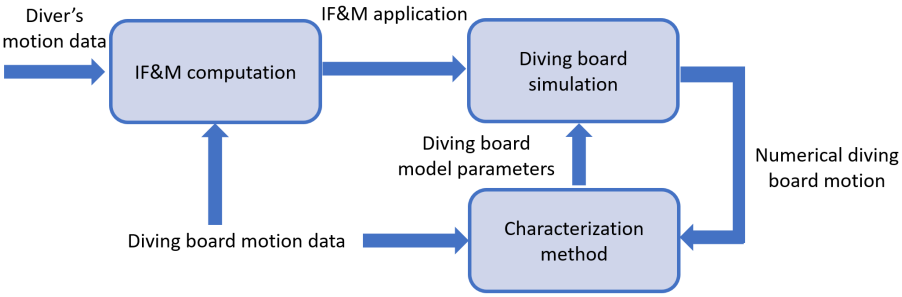

Fig. 2 Overview of the method based on diver's and springboard's motion capture inputs. The motion capture data are used to compute the interaction forces and moments, which are then applied to the diving board model. The diving board model parameters are determined by minimizing the discrepancy between the E&NVD

Motion capture data of diving trials gave the vertical displacement of the studied diving board and the diver's motion. A weak coupling between a finite element model of a diving board and a biomechanical model of the diver was carried out. The interaction forces and moments between the diver's feet and the diving board (IF&M) were computed using a motion-based ground reaction forces and moments (GRF&M) predictive method. This predictive method is an inverse dynamics one based on an optimization approach. The IF&M were applied on the diving board model. The diving board model effective parameters (material, geometry and contact) were finally identified using an optimization approach minimizing the discrepancy between the E&NVD (Fig. 2).

2.1 Experimental data

The motion capture data were recorded with the optoelectronic system Qualisys (12 12-Mpixels OQUS 7+ cameras, 200 Hz). A male recreational diver (1.65 m, 68 kg) was equipped with a set of 45 reflective markers placed on standardized anatomical landmarks as recommended by the International Society of Biomechanics [20, 21]. Fifty reflective markers were placed on the diving board sides, as shown in the Fig. 3 a). 49 markers were placed 10 cm apart on a side of the diving board. The 50th marker was placed on the other side at

the same distance (6 cm) from the diving board free end as the 49th marker. The participant signed an informed consent form in agreement with the ethical committee of Rennes 2 University (Reference 2022-006).

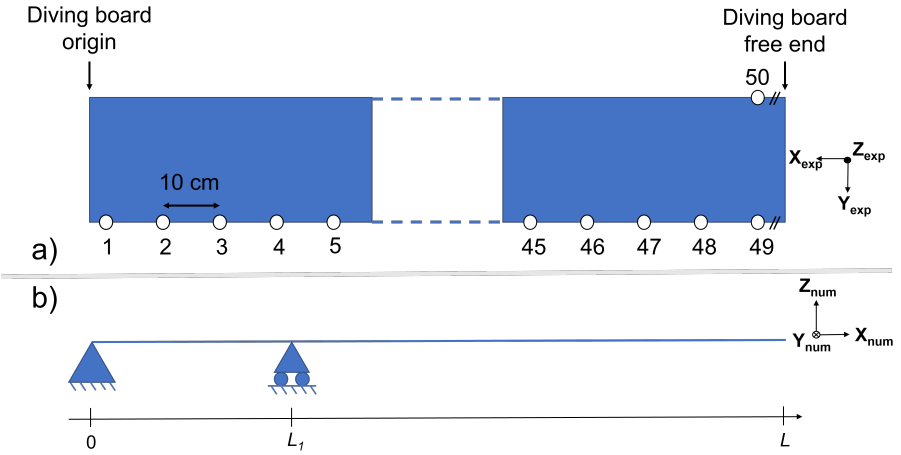

Fig. 3 a) Diving board markers location and experimental frame definition b) Diving board model and numerical frame definition

The experimental frame ($\boldsymbol{X_{exp}}$, $\boldsymbol{Y_{exp}}$, $\boldsymbol{Z_{exp}}$) was created from a reference (L-frame locating origin and axes of the experimental frame) placed at the diving board free end, which was slightly deflected because of the diving board self-weight. The line fitting the positions of the markers from the origin to the fulcrum of the diving board was considered as the absolute horizontal. An angle $\alpha = 0.9°$ between $\boldsymbol{X_{exp}}$ and this line was found.

A static trial of the diving board without any load, named reference trial, was recorded. It provided the reference $\boldsymbol{Z_{exp}}$-position of each marker, which was subtracted to the $\boldsymbol{Z_{exp}}$-position of each marker at each frame. The participant performed two RA (103C) and two SP (5111A) dives. The 5111A dives are supposed to be performed with a running approach, which was not the case here. The aim was to provide input data for dives with and without a running approach and not to study specific dives. One video for each type of dive is available as supplementary material (Online Resource 1 for the RA dive and Online resource 2 for the SP dive).

2.2 Diving board simulation

2.2.1 Diving board model

The diving board model was developed in the Matlab (Release R2021a, MathWorks, Inc., Natick, Massachusetts, United States) toolbox ATL4S [22]. The diving board was regarded as a 2D elastic Bernoulli beam with small deflections and was modeled as shown in Fig. 3 b). All the joints were assumed to

be point-wise. The unilateral contact between the diving board and the fulcrum at $X_{num} = L_1$ was managed with a linear complementary problem in the framework of non smooth contact dynamics [23], considering relative velocities between nodes in contact at fulcrum before and after rebound. The gravity effect was taken into account. The diving board model was meshed with 49 nodes, evenly spaced. Each node in the model corresponded to an experimental marker. A time increment equal to the experimental one (sampling frequency of 200 Hz) was used. The time integration was performed using the Euler-theta method ($\theta = 0.5$). The diving board model was considered static at the first time step. The motion capture was started when the diver and the diving board seemed to be static. Due to occlusion of diver markers in the labellization process, the beginning of the four studied dives was omitted and the first experimental time step took place during the diver and diving board motions. To have an experimental initial condition close to a static state, the trials were cut so that the velocity of the 49th marker at the first time step was less than 0.01 $m.s^{-1}$.

The diving board model was characterized by the following parameters:

- the Young's Modulus E (Pa);
- the density ρ ($kg.m^{-3}$);
- the thickness h (m) (according to $\boldsymbol{Z_{num}}$);
- the coefficient of restitution e.

The coefficient of restitution is a value between 0 and 1 quantifying the energy dissipation due to the contact with the fulcrum. This is the only source of energy dissipation in the model. The diving board width b (according to $\boldsymbol{Y_{num}}$) was set to 0.5 m.

2.2.2 IF&M computation

IF&M were computed by applying motion capture data to a biomechanical model of the diver. All the following steps were realized in the Matlab toolbox CusToM [24]. The diver model was composed of 18 segments and 44 degrees of freedom. Its geometry was scaled to the participant thanks to the studied trial data and the method described in reference [25]. The body segment inertial parameters of the model were computed as presented in reference [26]. For each trial, inverse kinematics were performed to obtain the joint angles corresponding to the participant's motion. The obtained evolution of joint coordinates were filtered with a 4th-order Butterworth low-pass filter with no phase shift and a cutoff frequency of 10 Hz [27].

The IF&M were then computed using a motion-based GRF&M prediction method adapted from reference [28]. This method consisted in two steps at each frame: contact detection and forces distribution. Each foot of the participant was mapped with 14 points, named prediction points (PP), as presented in Fig. 4. The contact detection step identified all the active PP in contact with the ground using positions and velocity thresholds. A maximal force equal to 0.4 Body Weight (BW) was allocated to each active PP [29]. As up to 28

Fig. 4 PP defined on the biomechanical model. Issued from [28]

PP may be active, a resulting force of up to 11.2 BW may be obtained. The forces distribution step distributed the GRF&M among all active PP using an optimization approach constrained by the participant's dynamic equilibrium.

The initial method was extended to studies involving interaction with a moving or non-horizontal structure or both, considered as a single rigid solid [30]. A frame linked to the structure (O_m, $\boldsymbol{X_m}$, $\boldsymbol{Y_m}$, $\boldsymbol{Z_m}$) was created using the 3D displacements of three additional markers placed on it. These markers were used to define the structure plane (O_m, $\boldsymbol{X_m}$, $\boldsymbol{Y_m}$). $\boldsymbol{Z_m}$ was defined as the normal to the structure plane. At each frame, a transformation matrix from the global frame to the structure frame was computed and used to express the relative positions of the PP in the structure frame. The relative velocity of each PP in the structure frame was defined as the difference between the absolute velocity of the PP and the absolute velocity of O_m. The active PP were identified using relative positions and velocity thresholds.

The diving board was regarded as a series of rigid surfaces. The existing contact detection step included a new sub-step to identify the diving board surface under the participant's feet among the whole diving board, named potential contact surface (PCS) (Fig. 5). At each frame and for each PP, the number of the diving board marker which was closest to the considered PP was saved. The PCS was the surface between the first and the last markers found previously. O_m was the point corresponding to the first marker of the PCS. The local frame ($\boldsymbol{X_m}$, $\boldsymbol{Y_m}$, $\boldsymbol{Z_m}$) was created from the PCS markers and the vector from the 49th to the 50th diving board. In addition to the position and velocity thresholds existing in the previous methods, the active PP had to be placed between the position of the first and the last PCS markers according to $\boldsymbol{X_m}$ and between 0 and the diving board width according to $\boldsymbol{Y_m}$.

2.2.3 IF&M application to the diving board model

The resulting IF&M in the plan ($\boldsymbol{X_{exp}}$, $\boldsymbol{Z_{exp}}$) were applied to the diving board model:

- the $\boldsymbol{X_{exp}}$-force component $\boldsymbol{FX}$;
- the $\boldsymbol{Z_{exp}}$-force component $\boldsymbol{FZ}$;

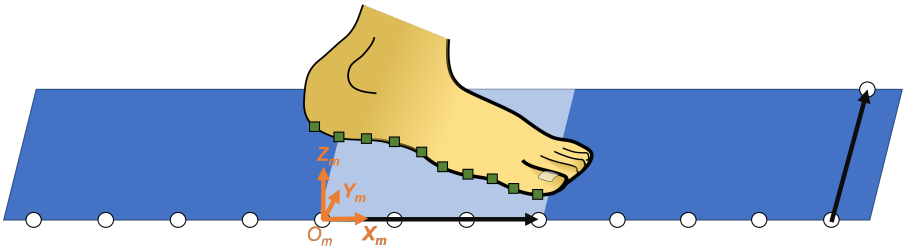

Fig. 5 Creation of the PCS frame (O_m, $\boldsymbol{X_m}$, $\boldsymbol{Y_m}$, $\boldsymbol{Z_m}$). Markers - rounds, schematic PP - squares, intermediate vectors - arrows, PCS - surface under the foot

- the $\boldsymbol{Y_{exp}}$-moment component $\boldsymbol{MY}$.

The IF&M from the two feet were summed and applied on an application point. The position of the center of pressure (CoP) under the participant's feet was computed at each time step using the positions and the vertical forces applied on the active PP [31]. The inclination of the diving board was not taken into account to compute the CoP positions. That is why the vertical forces were considered and not the forces normal to the diving board surface. The closest marker to the CoP among the part of the PCS in contact with active PP was considered as the application point (Fig. 6). Because of predicted IF&M filtering, non-zero IF&M could be found at time steps with no active PP. To avoid applying IF&M coming from filtering, the IF&M were set to 0 when there was no active PP.

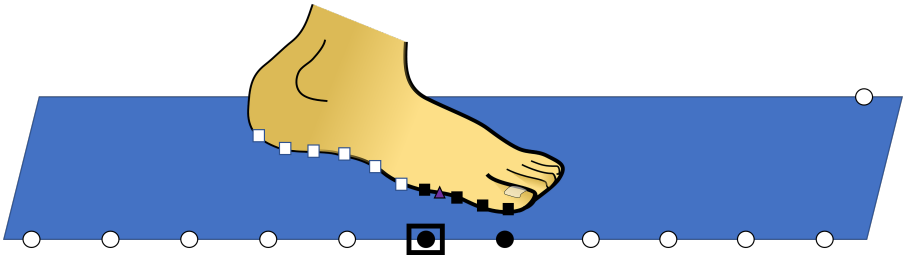

Fig. 6 Identification of the IF&M application point (black round in a black square). Active PP - black squares, inactive PP - white squares, PCS markers in contact with the active PP - black rounds, CoP - triangle, other markers - white rounds.

The moments $\boldsymbol{MY}$ for each foot obtained from CusToM were expressed at the experimental frame origin. They were transported to the heel points in alignment with the ankles. An angle of 0.11°between $\boldsymbol{X_{exp}}$ and $\boldsymbol{X_{num}}$ around $\boldsymbol{Z_{num}}$ was computed using the reference trial. It was considered as insignificant and not taken into account. Because of the angle α between $\boldsymbol{Z_{exp}}$ and $\boldsymbol{Z_{num}}$, the force vector was projected on $\boldsymbol{X_{num}}$ and $\boldsymbol{Z_{num}}$. $\boldsymbol{X_{exp}}$ and $\boldsymbol{Y_{exp}}$ were in the opposite direction from $\boldsymbol{X_{num}}$ and $\boldsymbol{Y_{num}}$ (Fig. 3). So the opposite of $\boldsymbol{FX}$ and $\boldsymbol{MY}$ were considered as the IF&M applied on the participant's feet.

The initial displacements $\boldsymbol{U}$ of the diving board model were computed as follows:

$$\boldsymbol{U} = \boldsymbol{K^{-1}F} \tag{1}$$

where $\boldsymbol{K}$ is the stiffness matrix and $\boldsymbol{F}$ the efforts matrix.

2.3 Characterization method

Initial parameters were defined as follows:

- $E_0 = 69.10^9$ Pa;
- $\rho_0 = 2.7.10^3$ kg.m^{-3};
- $h_0 = 0.05$ m;
- $e_0 = 1$.

E_0 and ρ_0 correspond to material properties of aluminium because diving boards are mostly made of aluminium alloy. h_0 was equal to the thickness measured on the origin of the diving board. e_0 induced no energy dissipation.

The normalized root mean squared error between the E&NVD 2 was minimized to characterize the diving board model:

$$\begin{aligned}\phi(E,\rho,h,e) &= \frac{1}{\phi_0}\sum_{i=1}^{n_t}\sum_{m=F+1}^{n_m}\frac{1}{n_e^i A_m^i}\sqrt{\sum_{k=1}^{n_e^i}(U_{exp}^i(x_m,t_k)-U_{num}^i(x_m,t_k))^2}\\ \phi_0(E_0,\rho_0,h_0,e_0) &= \sum_{i=1}^{n_t}\sum_{m=F+1}^{n_m}\frac{1}{n_e^i A_m^i}\sqrt{\sum_{k=1}^{n_e^i}(U_{exp}^i(x_m,t_k)-U_{num}^i(x_m,t_k))^2}\end{aligned} \tag{2}$$

where n_t is the number of trials, F the number of the marker closest to the fulcrum position (here 21), n_m the number of markers/nodes, n_e^i the number of time increments of the trial i, A_m^i the maximal experimental vertical displacement of the trial i at the abscissa x_m, U_{num}^i and U_{exp}^i the E&NVD at a given abscissa x_m and a given time t_k respectively for the trial i. The vertical displacements before the fulcrum were not taken into account because they were of the same order of magnitude as the optoelectronic system accuracy.

The optimization problem 3 was solved using a simulated annealing method:

$$\begin{aligned}&\min\ \phi(E,\rho,h,e)\\ &\text{subject to}\ \begin{cases}1.10^8\ \text{Pa} < E < 1.10^{12}\ \text{Pa}\\ 10\ \text{kg.m}^{-3} < \rho < 1.10^6\ \text{kg.m}^{-3}\\ 0.01\ m < h < 0.1\ m\\ 0 < e < 1\end{cases}\end{aligned} \tag{3}$$

The temperature T of the simulated annealing method was updated following the equation 4:

$$T = \frac{T_0}{log(k)} \tag{4}$$

where T_0 is the initial temperature (here 200) and k the iteration number.

2.4 Data analysis

The simulated annealing is a stochastic method so it may lead to results corresponding to different local minima. The characterization method described previously was run 50 times, which led to 50 different sets of parameters (a common parameter set for the four trials). A cluster analysis was performed on these 50 computational runs to determine how many groups of solutions there were among them. The squared Euclidean distance was used to perform the cluster analysis. The Calinski-Harabasz criterion was used to determine the optimal number of clusters for the studied runs.

The set of parameters obtained from a given run (E, h, ρ and e) were presented as $\frac{EI}{b}$ (where I is the second moment of area), ρ and e. Indeed, both the Young's modulus and the thickness affect the diving board stiffness.

Different metrics were used to analyse a trial among a given run. The metrics were all computed for each diving board node/marker after the fulcrum. The absolute error between the E&NVD at each frame was considered. The mean (solid line) and standard deviation (area around the solid line) values of the absolute errors were computed. This error was also normalized by A^i_m. The normalized cross correlation between the E&NVD was computed. The maximal correlation and the delay to obtain it were presented on the same graph. All these metrics were presented as functions of position along the diving board (abscissa X).

3 Results

Each run lasted between 30 minutes and an hour. As the computation of each run is independent of the others, the computation can be parallelized.

It was found that the optimal number of clusters was 1, so all the solutions were in the same group. In that case, the run leading to the lowest value of ϕ among the 50 runs was selected to present the results. The selected run led to $\phi = 0.58$ and the following parameters:

- $\frac{EI}{b} = 2.65.10^5$ Pa.m^3;
- $\rho = 855$ kg.m^{-3};
- $e = 0.099$.

Due to the assumptions made in the model (constant thickness, full and rectangular cross-section, no holes at the diving board free end), the obtained parameters are not expected to be close to those of an aluminium alloy. They are effective parameters suitable for our case study.

The maximal absolute errors between the experimental and numerical displacements at the diving board free end were 0.23 m (49 % of A^1_{49}) and 0.24 m (52 % of A^2_{49}) for the RA dives. The same results for the SP dives were 0.29 m (58 % of A^3_{49} and 59 % of A^4_{49}). The maximal errors were observed between touchdown and takeoff for the four dives. At the fulcrum position, the same results were 0.055 m (70 % of A^1_F) and 0.051 m (65 % of A^2_F) for the RA dives.

The same result for the SP dives were 0.047 m (59 % of A_F^3) and 0.033 m (43 % of A_F^4). These maximal errors were observed after takeoff for all the dives.

The mean values of the absolute error increased as the abscissa increased for all the trials. The maximal mean absolute errors were 0.065 m and 0.045 m for RA dives; 0.054 m and 0.060 m for SP dives. For the SP dive 3, the maximal normalized error was observed at the diving board free end. For the three other dives, the maximal normalized errors were observed between $X = 3,0$ m and $X = 3,1$ m. These maximal errors had values of 22.3 % and 12.2 % for RA dives; 10.9 % and 12.5 % for SP dives. For both the absolute and normalized errors, the standard deviation values increased as the mean values increased for all the dives.

The maximal correlation increased as the abscissa increased for all the dives. The associated delay decreased as the abscissa increased for RA dives. The opposite observation was made for the SP dive 3 and no delay was observed for the SP dive 4. The maximal correlations were between 0.88 and 0.96 for all the dives. The maximal delays were between 0 s (no delay for the SP dive 4) and 0.015 s for all the dives.

The graphics corresponding to the used metrics (Fig. 7) and the evolution of vertical displacements (Fig. 8) are presented for the trial with the lowest maximal mean absolute error and normalized absolute error (trial 2, which is a RA dive). The first time step in Fig. 8 corresponds to the first one with a vertical velocity of the 49th marker less than 0.01 $m.s^{-1}$ in the studied trial. For sake of clarity, similar figures for the other trials are available as supplementary material (Online Resource 3).

4 Discussion

4.1 Method accuracy

Since the diving board was not instrumented, the computed IF&Ms were not directly assessed. Nevertheless, reference [7] observed a peak reaction force on the springboard of 4 BW during a simulated reverse $3\frac{1}{2}$ tuck performed by a world class diver (RA dive). In the current study, 4 BW of the participant was 2668 N. The peak vertical forces observed during the RA dives were 3400 N and 3379 N, which corresponds to about 5 BW. Therefore, we obtained the same order of magnitude as the literature for the vertical reaction force, which seems to show that the IF&M computation method is suitable.

All the metrics are consistent for all the trials of the selected run. The maximal absolute errors observed between the experimental and numerical vertical displacements (E&NVD) were quite important. Nevertheless, the absolute errors were often less than these maximal values throughout the dives, leading to mean values far from these maximal values. A maximal mean absolute error between 0.045 m and 0.060 m, and a maximal delay less than 0.015 s between the E&NVD seem to be suitable to study time synchronization between the diver and the diving board. Indeed, the highest frequency in the spectrum of

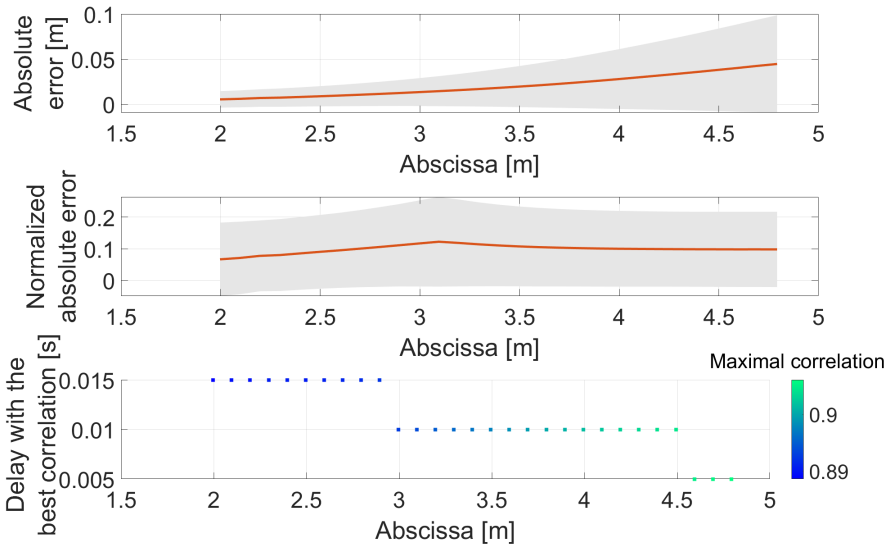

Fig. 7 Absolute error (up), normalized absolute error (in the middle) and cross correlation (down) for the selected trial

the vertical force of the RA dive 2 of the selected run was 4 Hz, which corresponds to a period of 0.294 s. The contact phase before the flight phase is a crucial phase of the dive [2, 7, 8, 11]. It is performed close to the diving board free end, where the considered errors are smaller, and lasts around 0.5 s [1, 32].

Previous models used in the literature led to smaller errors when considering vertical displacement. Reference [15] obtained an error between the E&NVD at the diving board free end of less than 5 cm throughout a RA dive using a mass-spring system model with decaying oscillations after the hurdle step. However, this model only considers the diving board free end which may be limiting for the study of RA dives during the running approach. The vertical mass-spring system to model the diving board free end results in a vertical reaction force acting on the diver [33]. The horizontal reaction force plays an important role in the generation of angular momentum and board clearance. The model used in reference [17] considers the rotation and the horizontal displacement of a part of the springboard whose location (and the associated parameters) can change during the dive. This model led to errors on the maximal deflection of less than 7 cm for the studied RA dives in reference [33], which is lower than those obtained in the present study. However, although this model takes into account the horizontal displacement of the springboard, its rotation and its interaction with the diver at different locations on the springboard, it only considers a part of the springboard at each frame. Our model considers the diving board as a whole throughout the dive. This is notably interesting to study the running approach which is also an important phase in

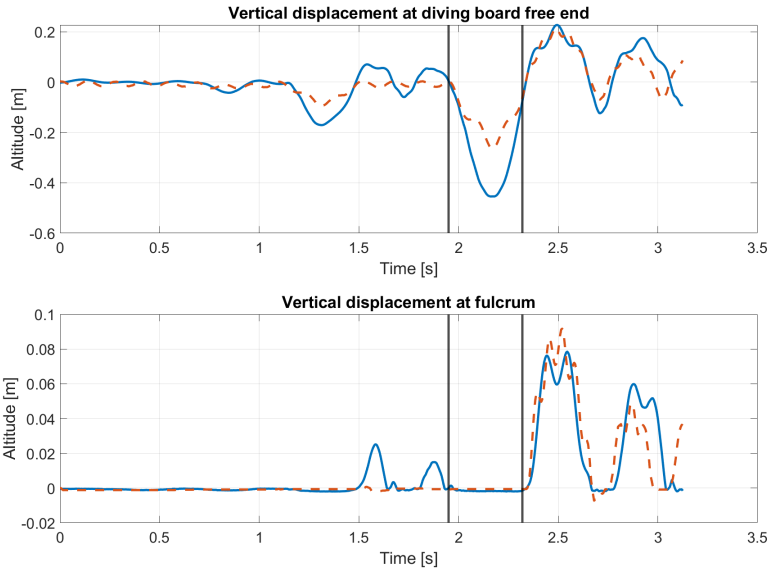

Fig. 8 Evolution of vertical displacement at diving board free end (up) and fulcrum (down). Experimental displacement in solid line. Numerical displacement in dashed line. Vertical lines represent touchdown and takeoff time steps

springboard diving performance [11]. The model presented here enables further studies of other mechanical features of the diving board as its energy and its interaction with the fulcrum notably during the hurdle step (from hurdle landing to hurdle touchdown in Fig. 1).

4.2 Limits and perspectives

The diving board model mesh was based on the experimental markers. It could be interesting to study the mesh impact on the characterization method results. A refined mesh may improve the method accuracy, whereas a coarser mesh may decrease the computation time.

It was assumed that the IF&M was applied on one point of the diving board. Vertical forces were used to compute the CoP positions. It would be more realistic to consider forces normal to the diving board and to compute the CoP positions in the frame linked to the diving board. Moreover, during the dives, the contact surface between the participant's feet and the diving board often contained multiple diving board markers. It could be interesting to study if the numerical displacements obtained with the optimal model could be closer to the experimental ones considering an IF&M distribution among several nodes of the diving board model.

Because of the stochastic feature of the method, 50 runs were carried out. The best run led to a suitable characterized model. The choice of 50 runs was made arbitrary. It could be interesting to perform an analysis to determine the

required number of runs to obtain at least one suitable set of parameters for the studied diving board. Moreover, a study on the influence of the parameters of the simulated annealing algorithm may help to know how to better explore the solutions space. Lastly, the presented study is based on four experimental trials performed by one participant. It would be interesting to study the impact of the amount of input data on the results accuracy.

The accuracy assessment of the characterization method was carried out using the trials used for the parameter determination. The accuracy assessment should be carried out using independent additional trials to obtain unbiased results. This choice was made because only four trials were recorded. Moreover, for a given set of trials to be studied, they could all be used in the characterization method in order to be as accurate as possible on the whole set.

The presented method is based on motion capture data, which are widely used for biomechanical analysis. Therefore, this technology may be successfully used to study both diver and diving board motion. Nevertheless, this analysis is often limited due to restricted field of view, light reflections, and heaviness of acquisition to reconstruction process, reducing its effectiveness in practice in a swimming pool environment. It could be interesting to improve the method to be suitable for other types of input data (markerless technologies, IMU...).

As the participant was a recreational diver, the technique used by expert divers would be different and may modify the mechanical load applied to the board. For example, an expert diver would achieve a takeoff closer to the diving board free end. Moreover, only one fulcrum setting was considered. Thus, more fulcrum settings may improve the generalization of the model. It will be thus possible to know more on how the diver's technique impacts the characterization method and whether modifying the fulcrum setting in the model with the same parameters is suitable or not. Lastly, the whole trials were used in the parameter determination, keeping the free regime of the diving board after takeoff. This choice was made to develop a general method throughout the studied dives. It may be expected that if a part of the dives is not studied, it can be removed from the recorded trials to obtain a more accurate model of the targeted phase of the dive.

5 Conclusion

To improve springboard diving performance, the study of the interaction between the diving board and the diver is crucial. An accurate model of the diving board is thus essential to go further in the study of this interaction. Using the presented method, a diving board model with a similar behaviour as the diving board studied experimentally was obtained. This method characterized the model using motion capture data of the diver and the diving board. This characterization method coupled with a biomechanical model of the diver and the IF&M throughout the dives are interesting tools to study the interaction between the diver and the diving board. All these tools may be used for

further studies about time synchronization and energy transfers between the diver and the diving board, which are key points in springboard diving performance. As the diving board is modelled as a whole, the considered studies can be performed notably for dives with a running approach.

6 Acknowledgements

This study is supported by the ANR within the framework of the PIA EUR DIGISPORT project (ANR-18-EURE-0022).

The authors wish to thank François May for his help in developing the IF&M computation method.

References

[1] Sayyah, M., King, M.A., Hiley, M.J., Yeadon, M.R.: Functional variability in the takeoff phase of one metre springboard forward dives. Human Movement Science journal (2020)

[2] Sinclair, P.J., Walker, C.A., Rickards, T.: Kinematic determinants of dive height in springboard diving. Movement and Sports Sciences - Science et Motricite **75**(1), 107–112 (2012)

[3] FINA: FINA DIVING RULES 2017-2021. Technical report (2017)

[4] Yeadon, M.R., Hiley, M.J.: The limits of aerial and contact techniques for producing twist in reverse $1\frac{1}{2}$ somersault dives. Human Movement Science, 390–398 (2019)

[5] Miller, D.I., Sprigings, E.J.: Factors influencing the performance of springboard dives of increasing difficulty. Journal of Applied Biomechanics **17**(3), 217–231 (2001)

[6] King, M.A., Kong, P.W., Yeadon, M.R.: Maximising forward somersault rotation in springboard diving. Journal of Biomechanics, 157–163 (2019)

[7] Sprigings, E.J., Miller, D.I.: Optimal knee extension timing in springboard and platform dives from the reverse group. Journal of Applied Biomechanics **20**(3), 275–290 (2004)

[8] Cheng, K.B., Hubbard, M.: Optimal compliant-surface jumping: a multisegment model of springboard standing jumps. Journal of Biomechanics **38**, 1822–1829 (2005)

[9] Cheng, K.B., Hubbard, M.: Role of arms in somersaulting from compliant surfaces: A simulation study of springboard standing dives. Human Movement Science **27**, 80–95 (2008)

[10] Barris, S., Farrow, D., Davids, K.: Do the kinematics of a baulked take-off in springboard diving differ from those of a completed dive. Journal of Sports Sciences **31**(3), 305–313 (2013)

[11] Sanders, R.H., Gibson, B.J.: Technique and timing in the womens forward two and one half somersault pike and mens three and one half somersault pike 3m springboard dives. Journal of Science and Medicine in Sport **3**(4), 434–448 (2000)

[12] Sprigings, E.J., Stilling, D.S., Watson, L.G.: Development of a Model to Represent an Aluminium Springboard in Diving. International Journal of Sport Biomechanics, 297–307 (1989)

[13] Miller, D.I., Osborne, M.J., Jones, I.C.: Springboard oscillation during hurdle flight. Journal of Sports Sciences **16**(6), 571–583 (1998)

[14] Miller, D.I., Jones, I.C.: Characteristics of maxiflex® model B springboards revisited. Research Quarterly for Exercise and Sport **70**(4), 395–400 (1999)

[15] Haake, S., Goodwill, S., Heller, B., Schoraha, D., Gomez, J.: Dynamic modeling of a springboard during a 3 m dive. In: Procedia Engineering, vol. 2, pp. 3299–3304. Elsevier Ltd, ??? (2010)

[16] Kooi, B.W., Kuipers, M.: The Dynamics of Springboards. Journal of Applied Biomechanics **10**(4), 335–351 (1994)

[17] Yeadon, M.R., Kong, P.W., King, M.A.: Parameter determination for a computer simulation model of a diver and a springboard. Journal of Applied Biomechanics **22**(3), 167–176 (2006)

[18] King, M.A., Kong, P.W., Yeadon, M.R.: Determining effective subject-specific strength levels for forward dives using computer simulations of recorded performances. Journal of Biomechanics, 2672–2677 (2009)

[19] Jones, I.C., Miller, D.I.: Influence of fulcrum position on springboard response and takeoff performance in the running approach. Journal of Applied Biomechanics, 383–408 (1996)

[20] Wu, G., Siegler, S., Allard, P., Kirtley, C., Leardini, A., Rosenbaum, D., Whittle, M., D D'Lima, D., Cristofolini, L., Witte, H., Schmid, O., Stokes, I.: ISB recommendation on definitions of joint coordinate system of various joints for the reporting of human joint motion—part I: ankle, hip, and spine. Journal of Biomechanics **35**(4), 543–548 (2002)

[21] Wu, G., Van Der Helm, F.C.T., Veeger, H.E.J., Makhsous, M., Van Roy, P., Anglin, C., Nagels, J., Karduna, A.R., McQuade, K., Wang,

X., Werner, F.W., Buchholz, B.: ISB recommendation on definitions of joint coordinate systems of various joints for the reporting of human joint motion—Part II: Shoulder, elbow, wrist and hand. Journal of Biomechanics **38**(5), 981–992 (2005)

[22] Grange, S.: ATL4S—A Tool and Language for Simplified Structural Solution Strategy. Technical report, GEOMAS INSA-Lyon (2021)

[23] Acary, V.: Projected event-capturing time stepping schemes for nonsmooth mechanical systems with unilateral contact and Coulomb's friction. Computer Methods in Applied Mechanics and Engineering **256**, 224–250 (2013)

[24] Muller, A., Pontonnier, C., Puchaud, P., Dumont, G.: CusToM: a Matlab toolbox for musculoskeletal simulation. Journal of Open Source Software, Open Journals **4**(33), 1–3 (2019)

[25] Muller, A., Germain, C., Pontonnier, C., Dumont, G.: A simple method to calibrate kinematical invariants: application to overhead throwing. In: ISBS-Conference Proceedings Archive, pp. 78–81 (2015)

[26] Dumas, R., Chèze, L., Verriest, J.-P.: Adjustments to McConville et al. and Young et al. body segment inertial parameters. Journal of Biomechanics **40**, 543–553 (2007)

[27] Skogstad, S.A., Høvin, M., Holm, S., Jensenius, A.R., Nymoen, K.: Filtering Motion Capture Data for Real-Time Applications. In: New Interfaces For Musical Expression (2013). https://www.researchgate.net/publication/247159959

[28] Muller, A., Pontonnier, C., Dumont, G.: Motion-based prediction of hands and feet contact efforts during asymmetric handling tasks. IEEE Transactions on Biomedical Engineering **67**(2), 344–352 (2020)

[29] Fluit, R., Andersen, M.S., Kolk, S., Verdonschot, N., Koopman, H.F.J.M.: Prediction of ground reaction forces and moments during various activities of daily living. Journal of Biomechanics **47**(10), 2321–2329 (2014). https://doi.org/10.1016/j.jbiomech.2014.04.030

[30] Demestre, L., Morin, P., May, F., Bideau, N., Nicolas, G., Pontonnier, C., Dumont, G.: Motion-Based Ground Reaction Forces and Moments Prediction Method for Interaction With a Moving and/or Non-Horizontal Structure. Journal of Biomechanical Engineering **144**(11) (2022). https://doi.org/10.1115/1.4054835

[31] Kajita, S., Hirukawa, H., Harada, K., Yokoi, K.: Introduction À La Commande Des Robots Humanoïdes, (2015)

[32] Miller, D.I., Zecevic, A., Taylor, G.W.: Hurdle preflight in springboard diving: A case of diminishing returns. Research Quarterly for Exercise and Sport **73**(2), 134–145 (2002). https://doi.org/10.1080/02701367.2002.10609002

[33] Kong, P.W.: Computer Simulation of the takeoff in Springboard Diving. PhD thesis, Loughborough University (2005). https://hdl.handle.net/2134/9051